

## Effect of Fluorocarbon Surfactant on Electroforming of Copper Nano-Powders

Zhongbao Luo, Yuchang Su<sup>\*</sup>, Shixiang Yue, Qiushan Yu, Rabigul Tursun and Jing Zhang

School of Materials Science and Engineering, Central South University, Changsha 410083, China

\*E-mail: [yhsu@csu.edu.cn](mailto:yhsu@csu.edu.cn)

*Received:* 13 November 2020 / *Accepted:* 8 December 2020 / *Published:* 31 December 2020

---

The electrodeposition behavior, morphology, and particle size of copper nano-powders prepared using fluorocarbon surfactants or fluorocarbon combined with non-ionic compound surfactants were characterized by linear sweep voltammetry, cyclic voltammetry, X-ray diffraction, and field emission scanning electron microscopy. Copper nano-powders prepared using fluorocarbon surfactant or fluorocarbon, non-ionic compound surfactants without added sulfuric acid did not adhere to the plate. The fine particle size of the copper powders, which was mainly influenced by the anionic fluorocarbon surfactant, ranged from 50 to 200 nm. The powder morphology mainly depended on the non-ionic surfactant, and the electrodeposition process was governed by diffusion. The cyclic voltammetry curve indicated that the cathode peak current density is inversely proportional to the plate surface coverage. The change of current density in the electrodeposition process was directly related to the current efficiency. The mechanism of the formation of copper nano-powders by microemulsion electrodeposition was established and explained.

---

**Keywords:** Fluorocarbon surfactant; copper nano-powders; linear sweep voltammetry; cyclic voltammetry

### 1. INTRODUCTION

Copper nano-powders possess excellent physical and chemical properties which make them useful in a wide range of applications including electronics, lubrication, and catalysis [1-6]. Preparation of copper nano-powders is achieved through either physical or chemical means. The physical method is simple and generates a high purity product, but it also involves specialized equipment, high energy consumption, and low product yield. Chemical methods are accomplished by several different approaches, and chiefs among them are liquid phase reduction [7,8], hydrothermal synthesis [9], and electrodeposition [10-12]. The latter is particularly appreciated for its ability to prepare many varieties of high purity metal powders that cannot be achieved by conventional methods. Additionally, the high

production efficiency, low cost, and low pollutant emissions [13-15] associated with electrodeposition make it well-suited for meeting the needs of continuous industrial production.

Many researchers have used copper sulfate solution under constant current or constant voltage conditions in order to prepare copper nano-powders via electrodeposition. The homogeneity and stability of the electrolyte are crucial for achieving high quality powders and continuous industrial production. Several reports have demonstrated that small additions of surfactant to the electrolyte have important effects on the cathode polarization and crystal nucleation, as well as powder particle size and shape [12,13]. These surfactants include polyvinyl pyrrolidone (PVP) [2,12,16], sodium dodecyl sulfate (SDS) [2,17,18,19], polyethylene glycol (PEG) [2,19], Polyols [20], cellulose [2], thiourea [2,12,21,22], alkylphenol sulfonate (APES) [12], and Tween [13]. However, none of these surfactants have successfully achieved very fine copper powders, since particle sizes are typically in the order of a micron. This is primarily because the surface tension in the electrolyte is not greatly reduced by these selected surfactants, which promotes larger micelle sizes [23] and in turn larger particle sizes. The powders are also difficult to be cleaned and collected due to a number of factors including the surfactants' high dosages, low solubilities in water, and low hydrophilic-lipophilic balances (HLBs). As a result, it is common for the copper powder surface to be coated in a large amount of organic matter. Large quantity of sulfuric acid [2,4,12,24] is also used in the aforementioned electrodeposition methods, however the high concentration of acid in the electrolyte severely corrodes the electrode plates. During the electrodeposition process, the copper powder readily adheres to the electrode plates, this requires the plates to be manually scraped on a regular basis. Otherwise, the deposited particles cannot be separated from the cathode plate surface and amass rapidly, impeding the formation of nano-sized powders. To solve this problem, many researchers have employed pulse current [25,26] or ultrasonic electrodeposition to lessen the copper powders' affinity to the plate, but these strategies are difficult to scale up for industrial production.

It has already been demonstrated that the addition of fluorocarbon and hydrocarbon chain surfactants can greatly reduce the surface tension of electrolyte solution [27,28] to decrease micelle size. Moreover, fluorocarbon surfactants possess high thermal stability, surface activity, and chemical stability [29]. Therefore, in this work fluorocarbon surfactant is combined with the non-ionic surfactants coconut oil fatty acid diethanolamide and Tween in order to improve the electrochemical properties of the electrolyte as well as powder morphology and particle size. The formation mechanism of powder is also discussed.

## **2. EXPERIMENTAL**

### *2.1 Materials*

The cathode and anode were made from cathodic copper sheets of 99.9 % purity. The reagents used include fluorocarbon surfactants (FS, 98 %), Tween (98 %), coconut oil fatty acid diethanolamide (6501, 98 %), copper sulfate pentahydrate ( $\text{CuSO}_4 \cdot 5\text{H}_2\text{O}$ , AR) and ethylene glycol ( $\text{C}_2\text{H}_6\text{O}_2$ , 98 %). The performed tests was shown in Table 1.

**Table 1.** The performed tests, the bath composition and results.

Experiment num.	CuSO <sub>4</sub> •5H <sub>2</sub> O	Other conditions	Current efficiency
1	25 g/L	—	46 %
2	25 g/L	0.5 g/L FS	48 %
3	25 g/L	0.5 g/L FS+5 g/L 6501+5 g/L C <sub>2</sub> H <sub>6</sub> O <sub>2</sub>	40 %
4	25g/L	0.5 g/L FS+5 g/L Tween+5 g/L C <sub>2</sub> H <sub>6</sub> O <sub>2</sub>	66 %

## 2.2 Preparation

The electrolyte was prepared through the mixing of copper sulfate pentahydrate and compounding surfactant. Then the prepared electrolyte was dispersed into the electrodeposition vessel and allowed to magnetic stirring for 30 min prior to electrodeposition. The electrolyte temperature was  $25 \pm 2$  °C. Two copper plates ( $\Phi 88 \times 2$  mm) served as the anode and cathode, which had a plate spacing of 1 cm. The anode and cathode plates were polished with SiC sandpaper in 600, 800, 1200, and 2000 mesh size. Then the plates were washed with distilled ethanol and water. The electrodeposition vessel consisted of a 2 L beaker, and the current was adjusted using a SOYI-25100M power supply. The current was always held constant during copper powders preparation. Electrodeposition time was set at 10 min, at which point the copper powders were filtered from the solution, cleaned, and dried in a vacuum oven at  $60 \pm 2$  °C.

## 2.3 Characterization

The phase distribution of the dried copper powders was analyzed by a Rigaku 2550 X-ray diffractometer. The morphology and particle size were studied using field emission scanning electron microscopy (FE-SEM). Image-Pro Plus software was used to calculate the particle size.

Linear sweep voltammetry (LSV) and cyclic voltammetry (CV) tests were performed on a CHI660E electrochemical workstation (CH Instruments, Shanghai) using a three-electrode system at  $25 \pm 2$  °C. The cathode consisted of copper sheet of 99.9% purity ( $S = 1 \text{ cm}^2$ ), while the anode consisted of a platinum plate. The reference electrode was the saturated calomel electrode (SCE). Plate spacing was 1 cm. The cathode was polished, ultrasonically cleaned with alcohol, rinsed with distilled water, and blown dry. The anode was polished with alumina polishing powder, then rinsed with deionized water and blown dry.

### 3. RESULTS AND DISCUSSION

#### 3.1 Cathodic polarization curve analysis

The cathode polarization responses of different electrolyte systems were measured at a scanning rate of 5 mV/s. Fig. 1(a)-(d) are cathodic polarization curves of different electrolyte systems.

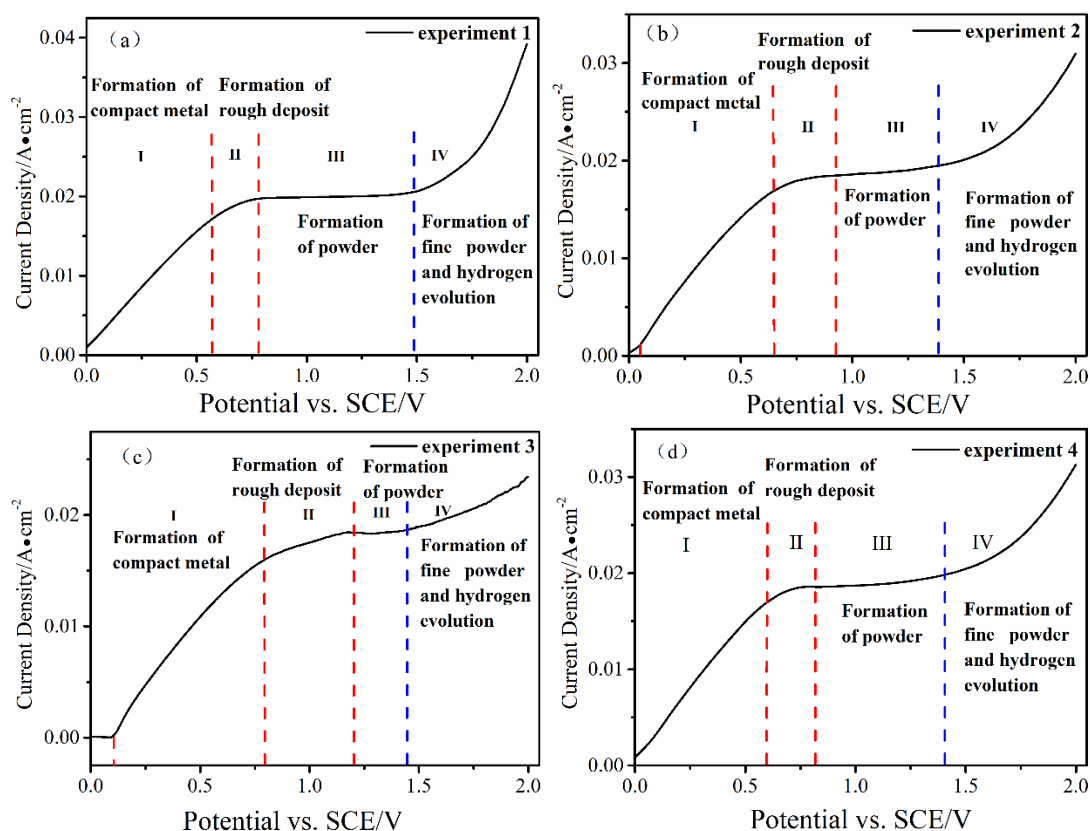


**Figure 1.** Cathodic polarization curves of different electrolyte systems. (a). 25 g/L  $\text{CuSO}_4 \cdot 5\text{H}_2\text{O}$ , (b) 25 g/L  $\text{CuSO}_4 \cdot 5\text{H}_2\text{O}$  + 0.5 g/L FS, (c) 25 g/L  $\text{CuSO}_4 \cdot 5\text{H}_2\text{O}$  + 0.5 g/L FS + 5 g/L 6501 + 5 g/L  $\text{C}_2\text{H}_6\text{O}_2$ , (d) 25 g/L  $\text{CuSO}_4 \cdot 5\text{H}_2\text{O}$  + 0.5 g/L FS + 5 g/L Tween + 5 g/L  $\text{C}_2\text{H}_6\text{O}_2$ .

The cathodic polarization curve can be divided into four parts [4, 30]. With increasing overpotential, current density increases rapidly in Regions I and IV as a result of controlled electrodeposition diffusion [31]. In Region III, increased overpotential has no obvious impact on the current density. The only fluctuations in this region are caused by Faraday current, and this process mainly depends on the solute diffusion. In Region III, the current density for the electrolytic liquid systems with surfactants added is lower than the corresponding surfactant-free system, which indicates that the additives have a strong inhibiting effect on copper deposition. In Fig. 1b, c, Region I exhibits a small platform at very low overpotential, and the current density increases slowly as overpotential further increases. By contrast, in Fig. 1a, d, the current density of Region I increases significantly with the increasing overpotential. This disparity is mainly attributed to the surfactant additives, which exhibit

strong adsorptive effects. When the surfactant forms an adsorption layer which covers the cathode surface, the metal ions must pass through the adsorption layer to reach the electrode surface and undergo the reduction reaction [32]. The adsorption of additives on the electrode surface can be represented by coverage,  $\theta$ . At a certain potential, the following formula applies [33]:

$$\theta = 1 - j/j_0 \tag{1}$$

Here,  $j$  and  $j_0$  are the current densities of the electrolyte with or without additives at the same overpotential, respectively. Since overpotential greatly influences the adsorption of surfactant, the effective overpotential [24] is used in calculations. As represented in Fig. 1b-c, at 1.38 V, the coverages of the electrolytic systems are 4.5 %, 9.9 %, and 3.5 %, respectively. Unlike the curves shown in Fig. 1b, c, the cathodic polarization curve shown in Fig. 1d lacks an obvious small platform in Region I. This is mainly due to the relatively low electrode surface coverage for this electrolyte system, which renders its resistance to metal ions inconspicuous. As shown in the cathodic polarization curve of Fig. 1c, Region IV of the relevant electrolytic system is associated with the highest coverage and lowest current density growth. Since this region mainly corresponds to the formation of powder, surfactant additives can reduce the efficiency of powder preparation. The current density at the effective overpotential in Fig. 1b-d are 0.1940, 0.0185, 0.0196 A/cm<sup>2</sup>, respectively. The current density in experiment 4 is the highest. the electrode reaction of  $Cu^{2+}$ , shown here [34]:



### 3.2 Cyclic voltammetry analysis

Cyclic voltammetry was used to study how different electrolyte systems impact the cathode peak current density and the cathode peak potential of the copper electrodeposition reaction. The cyclic voltammetry test was conducted across a voltage range of 0 to -2.5 V, and at a scanning rate of 0.02 V/s. The voltammograms of the systems are depicted in Fig. 2, where it is evident that all of the systems exhibit a cathode peak and lack an anode peak.

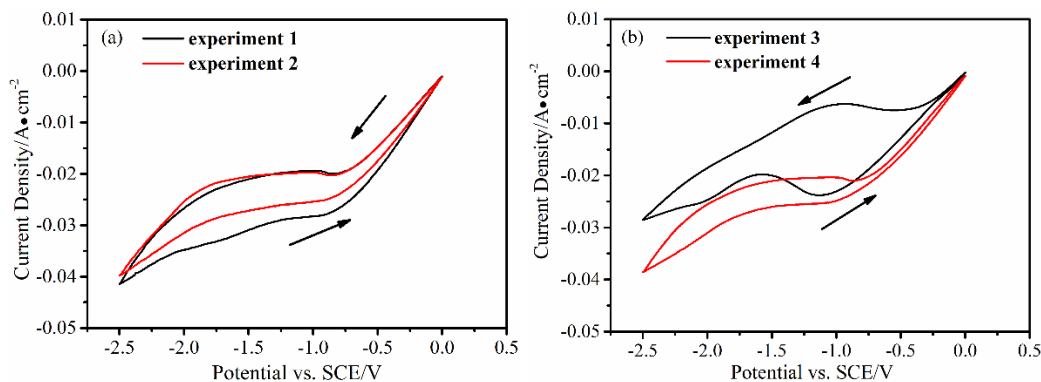


**Figure 2.** Cyclic voltammetry of different electrolyte systems.

This is indicative of irreversible charge transfer during the deposition process [32]. In Fig. 2, when the peak potentials of experiment 1 and 2 reach 0.91 and 0.89 V, respectively, the current density increases sharply with continued scanning, indicating the copper deposition process [35,36]. The corresponding peak current densities are 0.0278 and 0.0248 A/cm<sup>2</sup>, respectively. The peak potentials of experiment 3 and 4 are 1.21 and 1.06 V, respectively, while the corresponding peak current densities are 0.0238 and 0.025 A/cm<sup>2</sup>, respectively. The peak current densities of experiment 2, 3 and 4 are all lower than that of experiment 1, indicating that electrode surface coverage is improved for electrolytes that have been enhanced by FS or FS combined with 6501 or Tween. The improved surface coverage imparts greater resistance to the electrodeposition process. Fig. 2 shows that the cathode peak current density follows the trend of experiment 1 > 4 > 2 > 3. Therefore, cathode peak current density is inversely proportional to the electrode surface coverage. This result is consistent with the polarization curve analysis.

### 3.3 Effect of surfactant on powder morphology

Fig. 3 shows FE-SEM images of nano-copper powders prepared from different electrolyte systems at their current density corresponding to effective overpotentials.

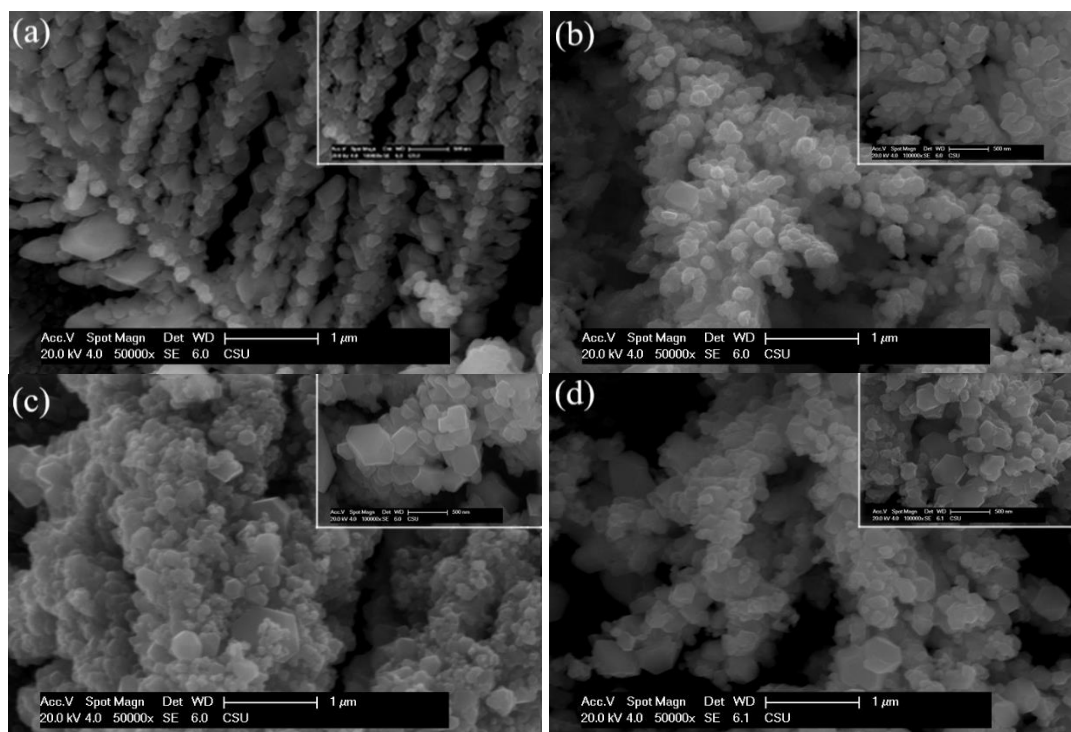


**Figure 3.** The morphology of electrodeposited copper powders: (a). current density 0.029 A/cm<sup>2</sup> (experiment 1) , (b). current density 0.026 A/cm<sup>2</sup> (experiment 2) , (c). current density 0.026 A/cm<sup>2</sup> (experiment 3) , (d). current density 0.029 A/cm<sup>2</sup> (experiment 4).

However, Fig. 5 shows neither the addition of surfactant nor surfactant type altered the preferred orientation of the crystal surface of copper deposition (111). XRD analysis indicates that each group

contains  $\text{Cu}_2\text{O}$ . The dendritic morphology observed in Fig. 3a is characteristic of the powder prepared from a surfactant-free electrolyte. Fig. 4 shows powder size is mainly distributed from 100 to 300 nm, with a small amount of larger particles. Fig. 3b shows nano-powder prepared with FS, which also exhibits a dendritic morphology. The particles are polydisperse, with sizes mainly distributed between 50 and 200 nm. The copper nano-powders shown in Fig. 3c was prepared using FS and 6501, with  $\text{C}_2\text{H}_6\text{O}_2$  as the auxiliary agent. The morphology is granular, and some particles are agglomerated and difficult to disperse.

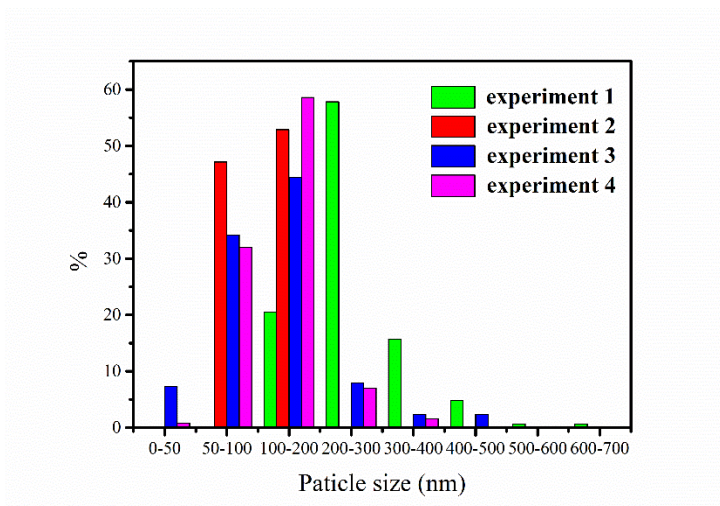


**Figure 4.** Particle size statistical analysis.

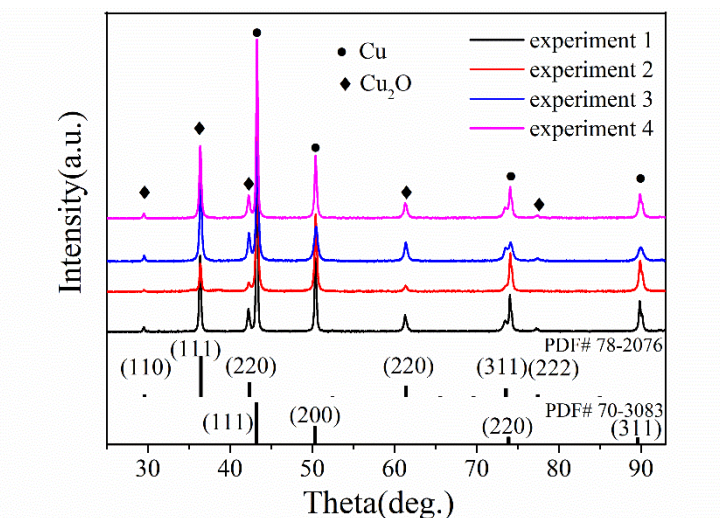


**Figure 5.** XRD analyses.

The same granular, somewhat agglomerated structures are observed in Fig. 3d, which shows copper nano-powder prepared using FS and Tween with  $\text{C}_2\text{H}_6\text{O}_2$  as the auxiliary agent. The particle sizes of both experiment 3 and 4 are primarily distributed between 50 and 200 nm. The comparable particle sizes observed for experiment 2, 3, and 4, as well as their significantly reduced size compared to the surfactant-free experiment 1, indicate that the particle size of powder mainly depends on the anionic FS.

This is primarily because FS or FS in combination with hydrocarbon chains can greatly reduce the surface tension of the electrolyte solution [26], thereby reducing the critical micellar solubility (CMC) and micellar radius, which is conducive to the formation of nanoparticles with small particle size [37]. Notably, Fig. 3b shows that the adding of FS to experiment 2 reduces the particle size, while the morphology is still dendritic. This can be explained by the long chain molecular structure of FS, which makes the formation of granular particles difficult. On the other hand, granular particles are easier to achieve when anionic FS is combined with either 6501 or Tween non-ionic surfactants, as depicted in Fig. 3c and 3d, respectively.

The current efficiencies of copper nano-powders prepared by different electrolyte systems are shown in Table 1. It is evident that higher plate coverage is correlated with lower current efficiency. According to the polarization curve analysis in Fig. 1, the current density of experiment 4 is the highest at the effective overpotential, which means the highest current efficiency (Table 1). According to the polarization curves, cyclic voltammetry curves and the current efficiencies in Fig. 1, 2 and Table 1, the change of current density in the electrodeposition process is directly related to the current efficiency, which indicates that the non-ionic surfactant has significant influence on the powder production. However, in Experiment 1, the copper powder adheres to the plate, hindering creating an obstacle to powder collection. Combining all of these results, the surfactant-free system has the low copper nano-powders yield. Therefore, the particle size of the prepared powder mainly depends on the anionic surfactant, and the powder morphology mainly lies on the non-ionic surfactant. This result is consistent with reported literature results [38].

### 3.4 Formation of copper nano-powders

Copper nano-powders prepared by experiment 1 readily adheres to the cathode plate. Therefore, in order to collect the powders, it must be scraped from the electrode surface.

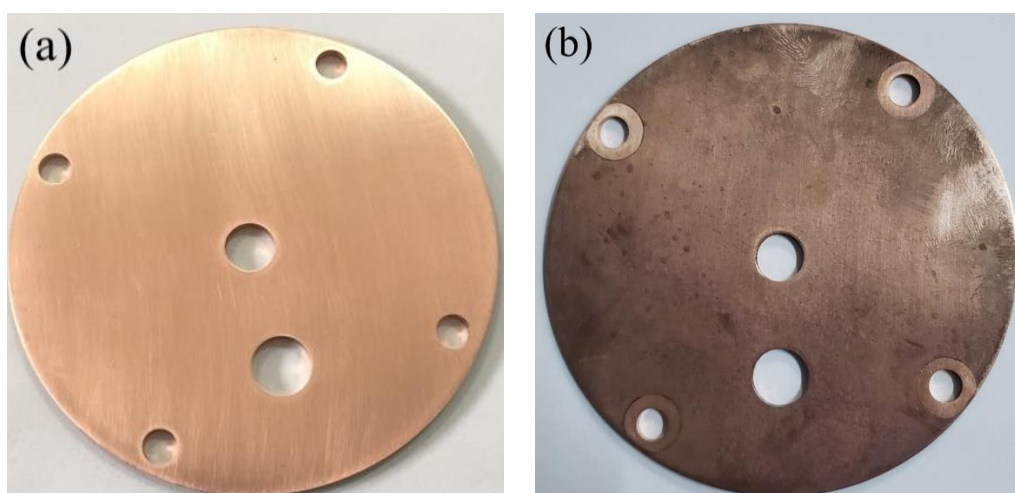


**Figure 6.** (a) Picture of cathode plate before electrolyte deposition, (b) Picture of cathode plate after electrolyte deposition.

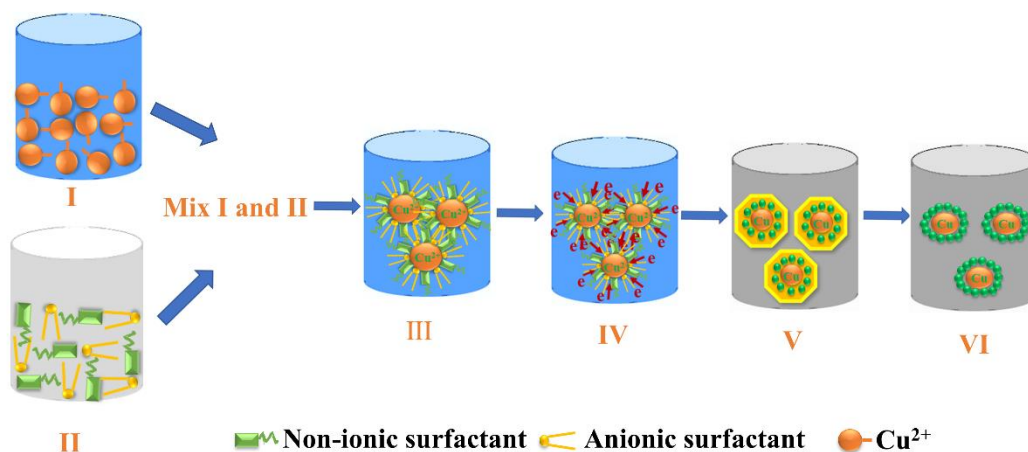


**Figure 7.** Schematic diagram of the formation of copper nano-powders by microemulsion electrodeposition.

Copper nano-powders prepared by experiment 1 readily adheres to the cathode plate. Therefore, in order to collect the powders, it must be scraped from the electrode surface. The copper nano-powders prepared by experiment 2, 3, and 4 do not adhere to the plate. This indicates that copper nano-powders prepared by adding FS or FS combined with non-ionic compound surfactants will not adhere to the cathode plate. Figs. 6 shows the cathode plate before and after the electrodeposition of experiment 4, respectively. Almost no copper powder adheres to the cathode plate after electrodeposition is complete.

In order to explore the formation mechanism of microemulsion electrodeposition, it is necessary to study the microemulsion microstructure. Under microemulsion-electrodeposition conditions, copper powder formation mainly consists of "nucleation-growth" stages [37]. Fig. 7 shows the formation mechanism of the electrolyte system consisting of FS and a non-ionic surfactant. The microemulsion (II) is combined with the copper sulfate solution (I), which induces ion exchange adsorption between  $\text{Cu}^{2+}$  and the anionic FS. The reduction reaction occurs within the micelle, imparting the microemulsion bead with a positive electrostatic charge (III). Due to the repulsion between the ionic surfactant's polar groups, pores exist on the formed micelles' surfaces [39]. Therefore, non-ionic surfactant additives may insert themselves into these pores. Non-ionic and ionic surfactants can cross-adsorb in the interfacial layer due to differences in the strength of polar hydrophilic groups, thereby increasing interfacial density and enhancing micelle membrane strength [11]. Once an electric current is applied, under the action of the cathode,  $\text{Cu}^{2+}$  is reduced to elemental copper in situ, rendering the micelle electrostatic charge negative (IV). Due to the thermodynamic instability of the electrolyte and the principle of minimum interfacial energy, surfactant molecules which adsorb on copper atoms collide with one another, causing deposition and coalescence of the electrolyte through the formation of a coating layer on the surface of the metal core (V). As the coating layer is electronegative, so is the cathode, and repulsion prevents the powder from adsorbing on the cathode plate. Therefore, The nano-copper powders prepared in this manner does not adhere to the electrode plate is achieved (VI). The collision of the copper-adsorbing

surfactant molecules causes the electrolyte to settle and coalesce. Throughout this process, the coating layer continuously exchanges materials with its environment [37]. The 6501 exhibits good solubility in water and an HLB value of 14. The micelle formed with FS in the presence of 6501 exchanges materials with the surrounding water molecules, making it difficult for the micelle to form a stable shape. As a result, the powder morphology is irregular. Tween has an HLB value of 9.3, such that Tween combined with FS can form relatively stable micelles. The number of nanoparticles comprising this powder is also increased compared to the FS-6501 system. C<sub>2</sub>H<sub>6</sub>O is also added to experiment 3 and 4 at a concentration of 5g/L to improve the dispersibility of the nano-copper powders. As a result, a large number of monodisperse particles can be observed under FE-SEM.

#### 4. CONCLUSIONS

We have successfully prepared nano-copper powders using fluorocarbon surfactant, both with and without non-ionic additives. The nano-copper powders prepared in this manner does not adhere to the electrode plate. Small particle size copper powders were achieved, in the range of 50 to 200 nm. Particle size was found to mainly depend on the presence of anionic fluorocarbon surfactant. The powder morphology mainly depends on the non-ionic surfactant. According to the polarization curve analysis, electrode coverage is inversely correlated to the current efficiency. Cyclic voltammetry demonstrated that the cathode peak current density is proportional to current efficiency and inversely proportional to the electrode surface coverage, and also that the electrodeposition is an irreversible process.

#### References

1. R. K. Nekouei, F. Rashchi and A. Ravanbakhsh, *Powder Technol.*, 250 (2013) 91.
2. R. K. Nekouie, F. Rashchi and N. N. Joda, *Powder Technol.*, 237 (2013) 554.
3. G. Orhan and G. Hapçı, *Powder Technol.*, 201 (2010) 57.
4. R. K. Nekouei, F. Rashchi and A. A. Amadeh, *Powder Technol.*, 237 (2013) 165.
5. A. Agrawal, S. Kumari, D. Bagchi, V. Kumar and B. D. Pandey, *Hydrometallurgy*, 84 (2006) 218.
6. K. K. Rani, Y. X. Liu, R. Devasenathipathy, C. Yang and S. F. Wang, *Ionics*, 25 (2019) 309.
7. M. Abdulla-Al-Mamun, Y. Kusumoto and M. Muruganandham, *Mater. Lett.*, 63 (2009) 2007.
8. M. Biçer and İ. Şişman, *Powder Technol.*, 198 (2010) 279.
9. S. Kubota, T. Morioka, M. Takesueb, H. Hayashic, M. Watanabe and L. S. J. Richard, *J. Supercrit Fluid.*, 86 (2014) 33.
10. V. M. Maksimovic', L. J. Pavlovic', M. G. Pavlovic' and M. V. Tomic', *J. Appl. Electrochem.*, 39 (2009) 2545.
11. W. He, X. C. Duan and L. Zhu, *J. Cent. South Univ. Technol.*, 16 (2009) 0708.
12. M. Quinet, F. Lallemanda, L. Ricq, J.Y. Hihn, P. Delobelle, C. Arnould and Z. Mekhalif, *Electrochim. Acta.*, 54 (2009) 1529.
13. J. Q. Xue, Q. Wu, Z. Q. Wang and S. F. Yi, *Hydrometallurgy*, 82 (2006) 154.
14. X. L. Xie, X. L. Zou, X. G. Lu, Q. Xu, C. Y. Lu, C. Y. Chen and Z. F. Zhou, *J. Appl. Electrochem.* 47 (2017) 679.
15. J. C. Niu, X.Y. Liu, K. D. Xia, L. L. Xu, Y. W. Xu, X. M. Fang and W. Lu, *Int. J. Electrochem. Sci.*, 10 (2015) 7331.

16. V. Sáez and T. J. Mason, *Molecule*, 14 (2009) 4284.
17. M. Y. Wang, Z. Wang and Z. C. Guo, *Nonferrous. Met. Soc. Chin.* 20 (2010) 1154.
18. X. F. Zhang, H. B. Yin, X. N. Cheng, K. M. Chen, H. F. Hu, Y. Q. and A. L. Wang, *Chin. J. Nonferrous Met.*, 16 (2006) 327.
19. L. Bonou, M. Eyraud, R. Denoyel and Y. Massiani, *Electrochim. Acta.*, 47 (2002) 4139.
20. R. S. Akpanbayev, B. Mishra, A. O. Baikonuroval and G. A. Ussoltseva, *Int. J. Electrochem. Sci.*, 8 (2013) 3150.
21. M. Quinet, F. Lallemand, L. Ricq, J. Y. Hihn and P. Delobelle, *Surf. coat tech.*, 204 (2010) 3108.
22. M. S. Kang, S. K. Kim, K. Kim and J. J. Kim, *Thin. Solid Films*, 516 (2008) 3161.
23. Z. O. Et-Tarhouni, E. Carter, D. M. Murphy, P. C. Griffiths, O. T. Mansour, S. M. King and A. Paul, *Colloids and Surfaces A: Physicochem. Eng. Aspects*, 492 (2016) 255.
24. N. D. Nikolic', K. I. Popov, L. J. Pavlovic' and M. G. Pavlovic', *J. Electroanal. Chem.*, 588 (2006) 88.
25. X. Xiao, B. Yan, J. M. Fu and X. M. Xiao, *J. Environ. Sci-China.*, 37 (2015) 163.
26. P. H. Britto-Costa and L. A. M. Ruotolo, *Hydrometallurgy*, 150 (2014) 52.
27. D. W. Kim, J. Y. Lee, S. M. Lee and J. C. Lim, *Colloid Surface A*, 536 (2018) 213.
28. A. Amell, C. Muller and M. Sarret, *Surf. Coat. Tech.* 205 (2010) 356.
29. Y. Y. Peng, F. Lu and Q. X. Tong, *Appl. Surf. Sci.*, 433 (2018) 264.
30. S. I. Jafar, *Eng. Tech. Journal.*, 27 (2009) 2308.
31. M. Sindhuja, V. Sudha, M. Abarna and S. Harinipriy, *Electrochim. Acta.*, 282 (2018) 750.
32. D. R. Lu, J. B. He, X. L. Li and Y. G. Zhu, *J. East. China Uni. of Sci. Technol.*, 30 (2004) 19.
33. J. Lipkowski and Z. Galus, *J. Electroanal. Chem.*, 61 (1975) 11.
34. H. Shen, H. C. Kima, M. Sunga, T. Limb and J. J. Kima, *J. Electroanal. Chem.*, 816 (2018) 132.
35. X. H. Guo, X. J. Zhou, X. H. Li, C. L. Shao, C. H. Han, X. W. Li and Y. C. Liu, *J. Colloid Interf. Sci.*, 525 (2018) 187.
36. W. B. Lou, W. Q. Cai, P. Li, J. L. Su, S. L. Zheng, Y. Zhang and W. Jin, *Powder Technol.*, 326 (2018) 84.
37. I. Capek, *Adv. Colloid Interfac.*, 110 (2004) 49.
38. S. X. Yue, Y. C. Su, Z.B. Luo, Q. S. Yu, R. Tursun and J. Zhang, *Mater. Sci Tech-logd.*, 50 (2019) 856.
39. M. J. Rosen and Q. Zhou, *Langmuir*, 17 (2001) 3532.